JSC-09836

NASA TECHNICAL MEMORANDUM

NASA TM X-58166
August 1975

A RADIATIVE TRANSFER MODEL FOR MICROWAVE EMISSIONS FROM BARE AGRICULTURAL SOILS

NATIONAL AERONAUTICS AND SPACE ADMINISTRATION

LYNDON B. JOHNSON SPACE CENTER

HOUSTON, TEXAS

1. Report No.	2. Government Accession No.	3. Recipient's Catalog No.
TM X-58166		

4. Title and Subtitle	5. Report Date
A RADIATIVE TRANSFER MODEL FOR MICROWAVE EMISSIONS FROM BARE AGRICULTURAL SOILS	6. Performing Organization Code

7. Author(s)	8. Performing Organization Report No.
William J. Burke, JSC and NRC, and Jack F. Paris, Lockheed Electronics Company and University of Houston	JSC-09836
	10. Work Unit No.

9. Performing Organization Name and Address	11. Contract or Grant No.
Lyndon B. Johnson Space Center Houston, Texas 77058	

12. Sponsoring Agency Name and Address	13. Type of Report and Period Covered
National Aeronautics and Space Administration Washington, D.C. 20546	Technical Memorandum
	14. Sponsoring Agency Code

15. Supplementary Notes

16. Abstract

A radiative transfer model for microwave emissions from bare, stratified agricultural soils was developed to assist in the analysis of data gathered in the Joint Soil Moisture Experiment. The predictions of the model were compared with preliminary X band (2.8 cm) microwave and ground based observations. Measured brightness temperatures at vertical (T_V) and horizontal (T_H) polarizations can be used to estimate the moisture content of the top centimeter of soil with ±1 percent accuracy. It is also shown that the Stokes parameters $[T_V + T_H]/2$ and $[T_V - T_H]$ can be used to distinguish between moisture and surface roughness effects.

17. Key Words (Suggested by Author(s))

- Microwave remote sensing
- Passive microwave observations
- Radiometric microwave observations
- Soil moisture
- Joint soil moisture experiment
- Passive microwave imaging system
- Multifrequency microwave radiometer
- Radiative transfer of microwaves

18. Distribution Statement

STAR Subject Category: 43 (Earth Resources)

19. Security Classif. (of this report)	20. Security Classif. (of this page)	21. No. of Pages	22. Price*
Unclassified	Unclassified	27	$3.75

*For sale by the National Technical Information Service, Springfield, Virginia 22151

CONTENTS

TABLES

FIGURES

Figure Page

A RADIATIVE TRANSFER MODEL FOR MICROWAVE EMISSIONS FROM BARE AGRICULTURAL SOILS

William J. Burke,* and Jack F. Paris†
Lyndon B. Johnson Space Center

SUMMARY

A radiative transfer model for the emission of microwave radiation from agricultural fields was developed. The predictions of the model are found to be in good agreement with preliminary data from the Phoenix Passive Microwave Imaging System observations. A sun angle effect observed in the L band data makes a simple comparison of the model with observations impossible at this time. An inversion of the model was capable of predicting the moisture content of the top centimeter of soil with an accuracy of approximately 1 percent. The model has been used to distinguish the microwave signatures of smooth and rough surfaces.

INTRODUCTION

The purpose of this memorandum is to present a theoretical model for radiative emissions from bare agricultural fields. The model utilizes the radiative transfer equation to calculate emissions from stratified soil in terms of brightness temperatures at vertical and horizontal polarizations as a function of look angle and moisture and temperature profiles of the soil. The model was developed to assist in the analysis of data from an aircraft experiment conducted during April, 1974. Data from the experiment have not been completely reduced. A small fraction (~1 percent) of the data have been reduced using by hand methods and are presented in a preliminary form. The data are used to verify the model and point out the capabilities and limitations of the model for analyzing radiometric data.

The first section gives an overview of the experiment and is followed by the development of the model and a comparison of its predictions with preliminary X band data. On the basis of this comparison an inversion is presented. A few words of caution are given concerning applications of the model to L band observations. A program listing of the model calculations is in the appendix.

---

*NASA Research Center.

†Lockheed Electronics Company and University of Houston.

THE SOIL MOISTURE EXPERIMENT

A feasibility test for detecting soil moisture using microwave remote sensing techniques was conducted under NASA auspices near Phoenix, Arizona April 5 and 6, 1974. Contributing investigators came from the Johnson Space Center, Goddard Space Flight Center, Agriculture Research Service of USDA, Environmental Research Institute of Michigan, University of Arkansas, University of Kansas, and Texas A&M University. X and L band radiometers were flown over four flight lines. Lines 1 and 2 are 32 kilometers (20 miles) long and alined north-south and lines 3 and 4 are 64 kilometers (40 miles) long, east-west alined. Three flights were made over the flight lines during the early afternoon of April 5 and a single flight at dawn April 6. At the time of the flights soil and temperature ground truth samples were taken from 95 16 hectares (forty acre) fields. Moisture samples were taken from the tops and bottoms of furrows at depths of 0 to 1, 1 to 2, 2 to 5, 5 to 9 and 9 to 15 cm at four points in each field. Temperature samples from the center of each layer were taken at one site per field. Soil samples were taken to the Agriculture Research Service Laboratory in Chickasha, Okalahoma for hygroscopic (ref. 1) and texture analysis. To measure the dielectric coefficients at X and L band frequencies samples of representative soil types were taken to Texas A&M University. To date, the dielectric coefficient analyses at X band have been completed but the L band have not.

The X and L band radiometers carried aboard the NASA P3A aircraft are the Passive Microwave Imaging System (PMIS) and Multifrequency Microwave Radiometer (MFMR). The PMIS (ref. 2) is a 10.69 GHz imaging radiometer that scans in 44 steps along an azimuthal arc of $\pm 34.5^\circ$ at a constant look angle of 49.5°. The antenna is a dual polarized cross slot array electronically stepped for scanning. Because of programming difficulties, PMIS data are not completely reduced. At the time of the April mission only the L band (1.42 GHz) component of MFMR was installed in the aircraft (ref. 3). The antenna is a flat plate dipole array whose look angle and polarization must be manually set. On the first afternoon and on the dawn flights the antenna was set at nadir look. The look angle was 40° for the second and third afternoon flights. Vertical and horizontal polarized brightness temperatures were measured on the respective flights. The MFMR data have been reduced.

MICROWAVE EMISSION FROM SOILS

This section discusses the problem of calculating the intensity of microwave emission measured by an antenna above an agricultural surface. Developing the radiative transfer model the following simplifying assumptions were made:

1. The radiation is incoherent

2. There is no attenuation or emission between the surface and antenna

3. The sky brightness is isotropic and has a value of 30°

4. Moisture and temperature are functions of depth only

5. Dielectric properties are constant across any given layer of soil

6. The surface of the soil is smooth

The extent these assumptions break down is discussed where the predictions of the model are compared with PMIS and MFMR data.

A cross section of a stratified soil is shown on figure 1. Layers have thicknesses ΔZ_j, which are not necessarily the same for all layers. The j th layer is banded on the top by the j th surface and by the j th surface on the bottom. Within this layer the dispersion relation for electromagnetic wave propagation is $k_j^2 = \left(\frac{\omega}{c}\right)^2 \mu_j \xi_j$. The frequency is ω in radians/sec, c the velocity of light, μ the magnetic permeability (assumed equal to one) and $\xi_j = \varepsilon_{Rj} + i\varepsilon_{Ij}$ is the complex dielectric coefficient. Written as $k_j = \frac{\omega}{c}(\beta_j + i\alpha_j)$, then

$$\left(\beta_{xj}^2 + \beta_{yj}^2 + \beta_{zj}^2\right) - \left(\alpha_{xj}^2 + \alpha_{yj}^2 + \alpha_{zj}^2\right) = \varepsilon_{Rj} \qquad (1)$$

$$2\beta_j \cdot \alpha_j = \varepsilon_{Ij}$$

Snell's law shows that the component of the wave vector parallel to the surface is a conserved quantity. Thus

$$\beta_{xj}^2 + \beta_{yj}^2 = \text{constant} = \text{Sin}^2\theta_o$$

and

$$\alpha_{xj} = \alpha_{yj} = 0$$

θ_o is the angle the ray emerges from the soil with respect to the surface normal. It ranges in value between 0 and 90°. Equation (1) reduces to

$$\beta_{zj}^2 - \alpha_{zj}^2 = \varepsilon_{Rj} - \text{Sin}^2\theta_o \qquad (2)$$

and

$$2\beta_{zj}\alpha_{zj} = \varepsilon_{Ij}$$

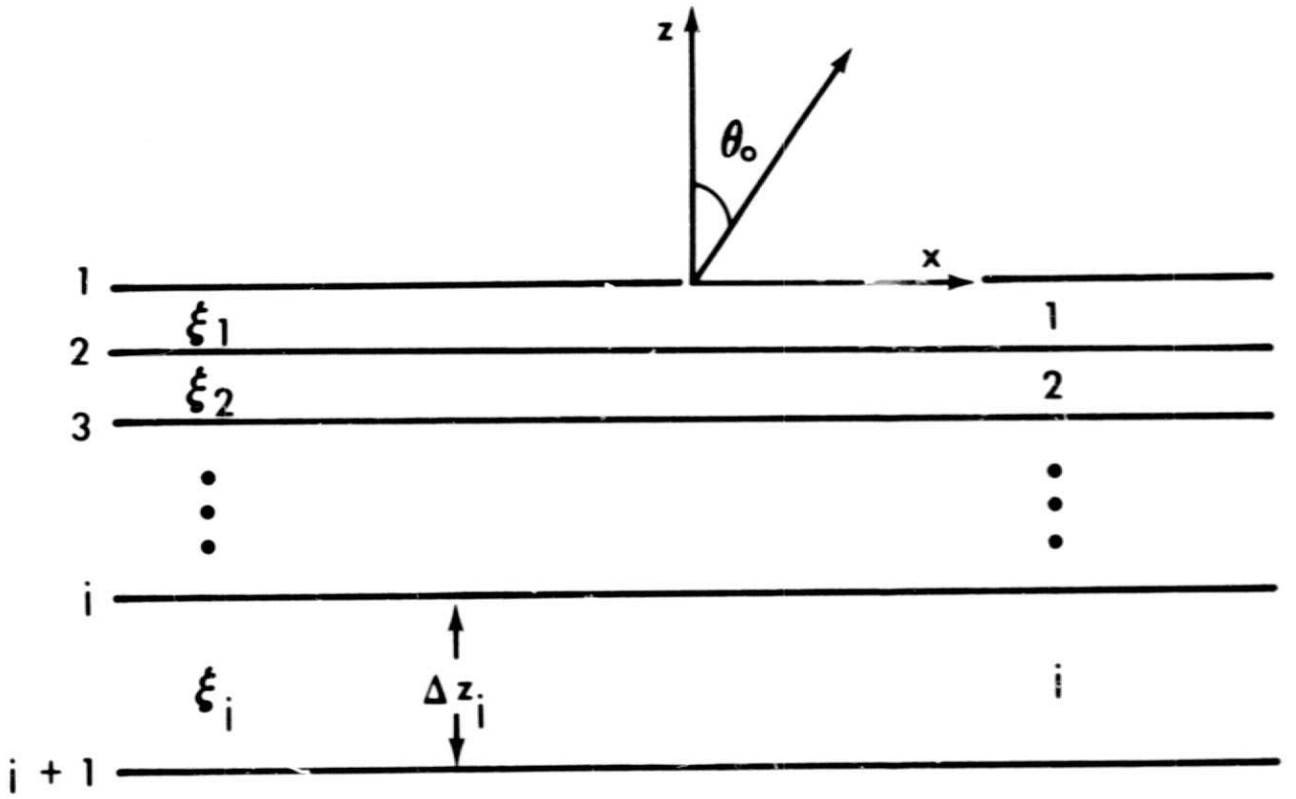

Figure 1.- Stratified medium used in development of emission model.

Solving

$$\beta_{zj} = \left[\frac{1}{2}\left(\varepsilon_{Rj} - \mathrm{Sin}^{2}\theta_{o}\right) \left(1+\sqrt{1+\frac{\varepsilon_{Ij}^{2}}{\left(\varepsilon_{Rj} - \mathrm{Sin}^{2}\theta_{o}\right)^{2}}}\right) \right]^{\frac{1}{2}} \qquad (3)$$

$$\alpha_{zj} = \varepsilon_{I}/2B_{zj}$$

At the boundary between the j and j-1 layers radiation is partially reflected and transmitted. The fractions of the incident electric field with horizontal and vertical polarizations reflected back into the j th layer are given by the Fresnel coefficients.

$$\rho_{H} = \frac{k_{zj} - k_{zj-1}}{k_{zj} + k_{zj-1}} \qquad (4)$$

$$\rho_{V} = \frac{\xi j-1\ k_{zj} - \xi j\ k_{zj-1}}{\xi j-1\ k_{zj} + \xi j\ k_{zj-1}}$$

where $k_{zj} = \beta_{zj} + i\alpha_{zj}$. Thus β_{z}, α_{z}, ρ_{H} and ρ_{V} all depend on the complex dielectric coefficient and angle θ_{o} that the ray emerges from the soil.

An attempt to construct a radiative transfer equation that describes radiation emitted from a stratified soil is now made. Within the first layer the radiative transfer equation is

$$\frac{d\ I_{\omega}}{d\ z} = -\gamma_{1}\ I_{\omega} + \gamma_{1}\ J_{\omega} \qquad (5)$$

γ is usually written as a product of the density and monochromatic mass absorption coefficient. By writing the Poynting theorem in an appropriate form it can be shown that $\gamma_{i} = 2\omega\alpha_{zi}(\theta_{o})/C$.

I_{ω} is the intensity of radiation at frequency ω. J_{ω} is the Planck emission function. In the microwave frequency range Planck's emission law reduces to the Rayleigh-Jeans approximation, where J_{ω} is proportional to the temperature of the medium T. Adopting a similar scaling rule for I_{ω}, and

effective temperature T_p can be defined which is directly proportional to I_ω. The subscript ω is suppressed and T_p refers to the intensity in a narrow range near ω. The subscript p refers to a polarization state. Since J_ω is isotropic and independent of polarization no designation is necessary. The radiative transfer equation in the first layer may be written

$$\frac{dT_p}{d\left(\gamma_i z\right)} = -T_p + T_i \tag{6}$$

This equation can be integrated from a point just below the surface to a point just above the interface between the first and second layers. Because the dielectric properties are assumed to be constant across the layer

$$T_p(1^-) = T_1\left(1 - e^{-\gamma_1 \Delta z_1}\right) + T_p\,(2^+)e^{-\gamma_1 \Delta z_1} \tag{7}$$

The argument $N^\pm$ implies that the measurement is made above (+) or below (-) the N th interface. The first term on the right hand side of equation 7 accounts for radiation emitted within the first layer and comes directly to the surface. The second term describes upwelling radiation at the bottom of the second layer. This in turn has two components: first, radiation emitted in the first layer and reflected at the interface between the first and second layers; and second, radiation transmitted from lower layers.

$$T_p\,(2^+) = R_{p2}\,T_1\left(1-e^{-\gamma_1 \Delta z_1}\right) + T_p\,(2^-)\left(1-R_{p2}\right) \tag{8}$$

R_{p2} is the absolute value squared of the Fresnel coefficient for p polarization (equation 4). The radiation field just above the surface is the value just below multiplied by the transmittance $(1-R_{p1})$

$$\begin{aligned} T_p(1^+) &= \left(1-R_{p1}\right) T_p\,(1^-) \\ &= \left(1-R_{p1}\right)\left\{T_1\left(1-e^{-\gamma_1 \Delta z_1}\right)\left(1+R_{p2}\,e^{-\gamma_1 \Delta z_1}\right)\right. \\ &\quad + \left(1-R_{p2}\right) T_p\,(2^-)\,e \end{aligned} \tag{9}$$

The radiative transfer equation can be integrated again to calculate $T_p(2^-)$. Repeating the procedure for N layers gives

$$T_p(1^+,\theta_o) = \sum_{i=1}^{N} T_i \left(1-e^{-\gamma_i(\theta_o)\,\Delta z}\right) 1+R_{p,i+1}(\theta_o)\, e^{-\gamma_i(\theta_o)\,\Delta_{zi}} \prod_{j=1}^{i} (1-R_{p,j}(\theta_o))\, e^{-\sum_{l=2}^{i} \gamma_{l-1}(\theta_o)\Delta z_{l-1}} \quad (10)$$

The brightness temperature measured by the antenna is the sum of the reflected sky brightness and radiation emitted from the soil

$$T_{B,p}(\theta_o) = T_{SKY}\, R_{p,1}(\theta_o) + T_p(1^+, \theta_o) \quad (11)$$

A computer program was written that used as its inputs the moisture and temperature profiles measured in the Phoenix fields. Dielectric coefficients were calculated using the soil type characteristic of each field with the polynomial representation given from Texas A&M measurements. With this information equation 11 could be calculated and results of the model compared with PMIS observations.

A COMPARISON WITH PRELIMINARY PASSIVE MICROWAVE IMAGING SYSTEM (PMIS) DATA

April 5 and 6, 1974 missions PMIS data have not been reduced to the point where average temperatures and standard deviations over fields are readily available. However, it is possible to take data from uncorrected printouts and estimate average temperatures by considering only data taken near the center of a field. The preliminary nature of average values cannot be overstressed. They do serve the useful purpose of helping to check the model's validity. The PMIS data are taken from lines 4 and 1 on the first flight of April 5 flight, and are given in Table I.

A program was developed, which takes the observed moisture and temperature profiles as well as soil types and calculates the horizontal and vertical brightness for the top and bottom of furrows in ten degree increments from 0 to 90°. A quick preliminary check of the specular model's applicability is to compare whether the predicted temperature at a look angle of 0° falls between the PMIS Tv and Th observations. No field failed to meet the minimal criterion.

TABLE I.- PMIS DATA FROM LINES 4 AND 1 ON THE FIRST FLIGHT APRIL 5, 1974

Field	Tv	Th	PM (1)
237	287	273	1.6
242	288	275	1.6
243	286	274	1.7
254	289	274	3.3
255	291	274	4.1
257	286	269	2.4
260A	283	267	4.4
261	287	272	3.3
264	286	274	2.8
299	281	266	2.5
300	285	266	2.3
317	288	251	1.7
334	284	272	1.4
102	277	266	
104	283	271	
106A	283	261	8.8
126	285	274	

Field 260A was selected to illustrate the capabilities of the model. Ground observations were simultaneous with the overpass. Average moisture and temperature profiles for the field are given in Table IIa. There is a wide difference between the moisture in the 0 to 1 cm layers of the top and bottom of furrows. Temperatures predicted by the model for the top and bottom of furrows are given in Table IIb. The temperature 272° K at 0° look angle from the top of the furrow lies between the PMIS T_V = 283° K and T_H = 267° K observations; the 225° K temperature of the furrows bottom does not. It is concluded that most of the radiation reaching the PMIS antenna comes from the top of furrows. Furrows in field 260A had a height of ~27 cm at a separation of 1 meter and were alined perpendicular to the flight line. Thus, significant shadowing of the bottom of the furrow is not a complete surprise.

TABLE IIa.- AVERAGE FIELD MOISTURE AND TEMPERATURE PROFILES

Field 260A

	Layer	Moisture	Temperature (°K)
Top	1	4.4	305.5
	2	10.8	303.7
	3	19.7	301.4
	4	21.6	297.3
	5	23.7	290.3
Bottom	1	12.8	304.4
	2	17.5	302.0
	3	21.1	299.2
	4	23.6	295.4
	5	23.0	289.3

TABLE IIb.- PREDICTED TEMPERATURES BY THE MODEL FOR TOP AND BOTTOM OF FURROWS

Field 260A

	Top		Bottom	
0°	Tv	Th	Tv	Th
0°	271.9	271.9	225.2	225.2
10°	272.4	271.2	225.7	224.9
20°	275.4	268.2	230.2	220.5
30°	280.4	262.6	238.0	212.6
40°	287.3	253.2	249.5	200.5
50°	295.6	238.3	265.0	181.2
60°	302.6	214.7	283.9	159.3
70°	299.3	177.5	300.8	127.1
80°	253.5	119.3	285.3	84.7
90°	30.0	30.0	30.0	30.0

Predicted temperatures from the top of furrows as a function of look angle are plotted on Figure 2. The straight lines marked T_V and T_H are PMIS observations. These curves intersect near a look angle of 30°. An inspection of data from the other fields show that with the exception of field 317, the intersection of predicted and observed temperatures occurs near 30°. Field 317 was a flat, smooth field. Here PMIS observations intersect the prediction curves near θ=50°. The conclusion is that surface roughness changes the effective look angle from 50 to 30°. Such an effect was anticipated by predictions of a rough surface emission model developed by Ulaby et al. (ref. 4). Their geometrical optics model predicts that as roughness increases the vertical emissivity is depressed and horizontal emissivity enhanced relative to the emissivity of a specular surface. Thus from a specular point of view, observations made at a look angle of 50° appear, to be made at a lesser angle. The apparent universality of the 30° observation suggests the roughness model can be inverted to determine the size of clods responsible for the X band emissions from Phoenix fields.

Two sets of calculations were made using varied layer patterns. For the first calculation temperature and moisture of the first two layers were averaged and combined. For the second calculation, all layers were set at a thickness of 0.5 cm. The temperature and moisture in each layer was set as the average of a linear interpolation across the layer; neither satisfied the zero look angle criterion as well as the ordinary profile.

AN ATTEMPT AT INVERSION

If a model is to be useful in remote sensing it must be capable of inversion. We must be able to go from aircraft observations to an estimate of the soil moisture. To effect such an inversion, the brightness temperatures of a set of pseudo-fields have been calculated. The temperature profile from top to bottom of these fields was set at $T_1 = 303$, $T_2 = 301$, $T_3 = 299$, $T_4 = 297$, $T_5 = 295$. The moisture profile was PM(1) = M, PM(2) = M + 2, PM(3) = M + 7, PM(4) = M + 14, PM(5) = M + 16. The dielectric coefficient is that of sandy clay. M was given values of 1 to 25 but the percent moisture in any given layer was not allowed to exceed 30 percent. This moisture profile is referred to as the ordinary profile. Other moisture profiles with sharper gradients were used. Unless otherwise specified we will be referring to model results using the ordinary profiles.

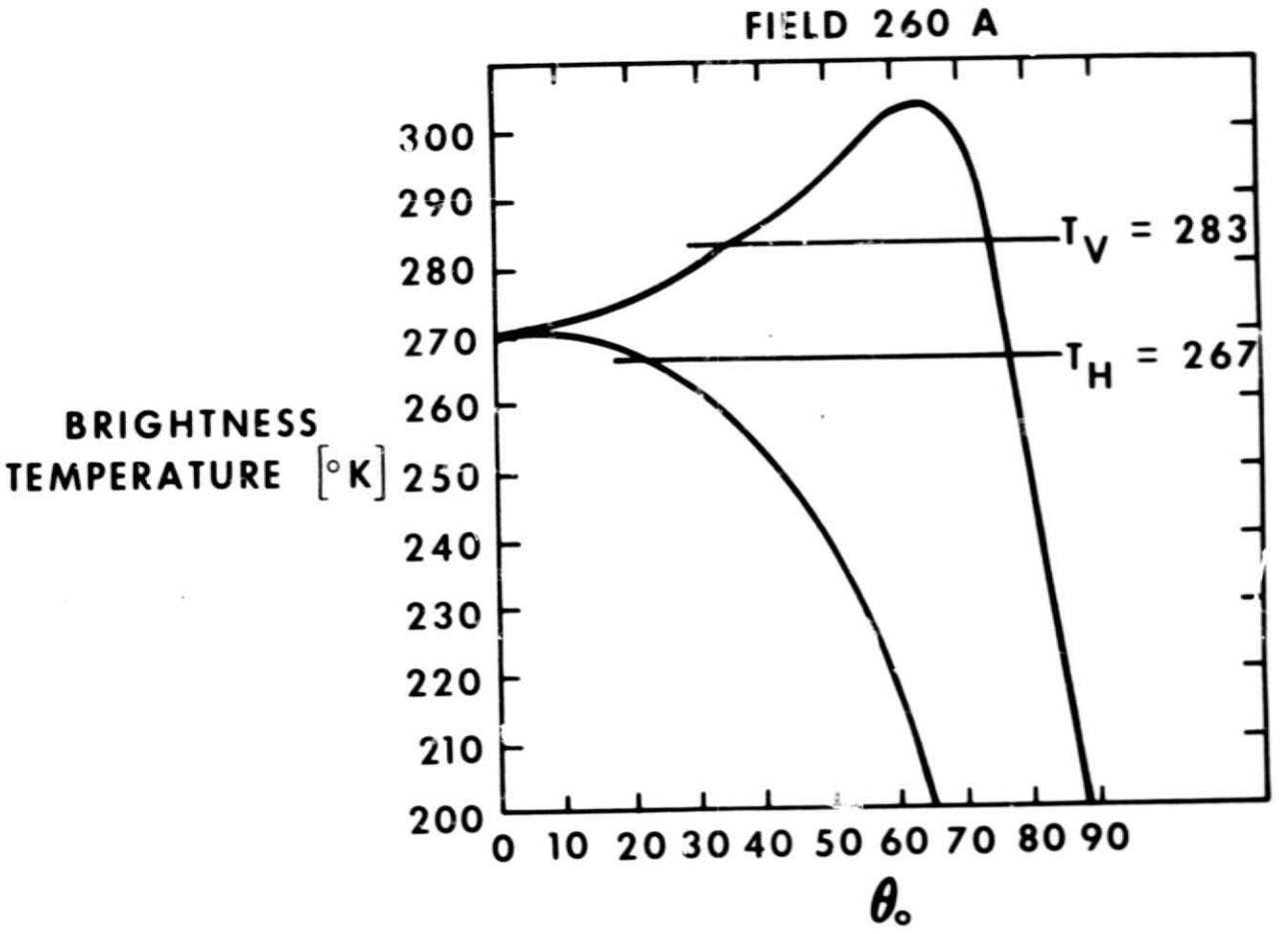

Figure 2.- Emission model predictions for Field 260A. The ascending curve is for vertical and the descending curve for horizontal polarizations. Straight lines marked Tv and Th are PMIS observations.

Values of calculated brightness temperatures as a function of the percent moisture in the first layer PM(1) are plotted on Figure 3 for look angles of 0, 30, and 50°. At the 0° look angle and PM(1) > 10 percent the average slope is -3.5° K/percent moisture. The slope tends to decrease at higher values of PM(1). For this reason it is thought that the model's predictions are consistent with the observations of a -3.3° K/percent moisture slope reported by Schmugge (ref. 1) for moistures up to 35 percent. Also the plot on Figure 3 can be used to attempt an inversion. Unless the presence of a flat field is indicated by the large separation between T_V and T_H, it is assumed that PMIS observations come from an effective look angle of 30°. The estimates gained by this method are found to vary by no more than 1 percent from the average values of PM(1) found in ground truth results.

The predicted difference between T_v and T_h as a function of PM(1) at look angles of 20, 30, 40 and 50° are plotted on Figure 4. A scatter plot of PMIS observed values of $T_V - T_H$ as a function of observed PM(1) is superimposed on the calculations. Average values of fields 317 A, B, C, D are found near the $\theta_o = 50°$ curve while the rest of the data points lie close to the $\theta_o = 30°$ curve.

Figure 5 is a plot of the average value of the vertical and horizontal brightness temperatures as a function of PM(1). The curves are for $\theta_o = 30°$ and 50°. We note that $1/2\ (T_V + T_H)$ is only slightly dependent on the surface roughness characteristics. A scatter plot of PMIS observations appears less correlated with the $1/2\ (T_V + T_H)$ predictions than with the $(T_V - T_H)$ predictions.

A plot of $(T_V - T_H)$ as a funciton of $1/2\ (T_V + T_H)$ for $\theta_o = 30$ and 50° is given on Figure 6. The nearly vertical curves are lines of constant moisture. A scatter plot of PMIS observations is also displayed. Data points taken from fields 313 and 296 appear on the graph. Aerial photographs show the fields were being irrigated during the overpass. No ground truth for these fields is available. The anomalous positions of the points on the graph suggest that the beam is made up of components from smooth water flowing in furrows and relatively dry tops of furrows. Signatures from a small pond and large metal building on line 4 are plotted. The pond is cool and flat but the metal building is cold with no appreciable polarization.

It should be pointed out that if $1/2\ (T_V + T_H)$ and $(T_V - T_H)$ should turn out to be significant parameters, it would not be a total surprise. Paris (ref. 5) has shown that these quantities are the non-zero components of the Stokes vector. Effectively the model sums up the contributions of the Stokes vector for each layer.

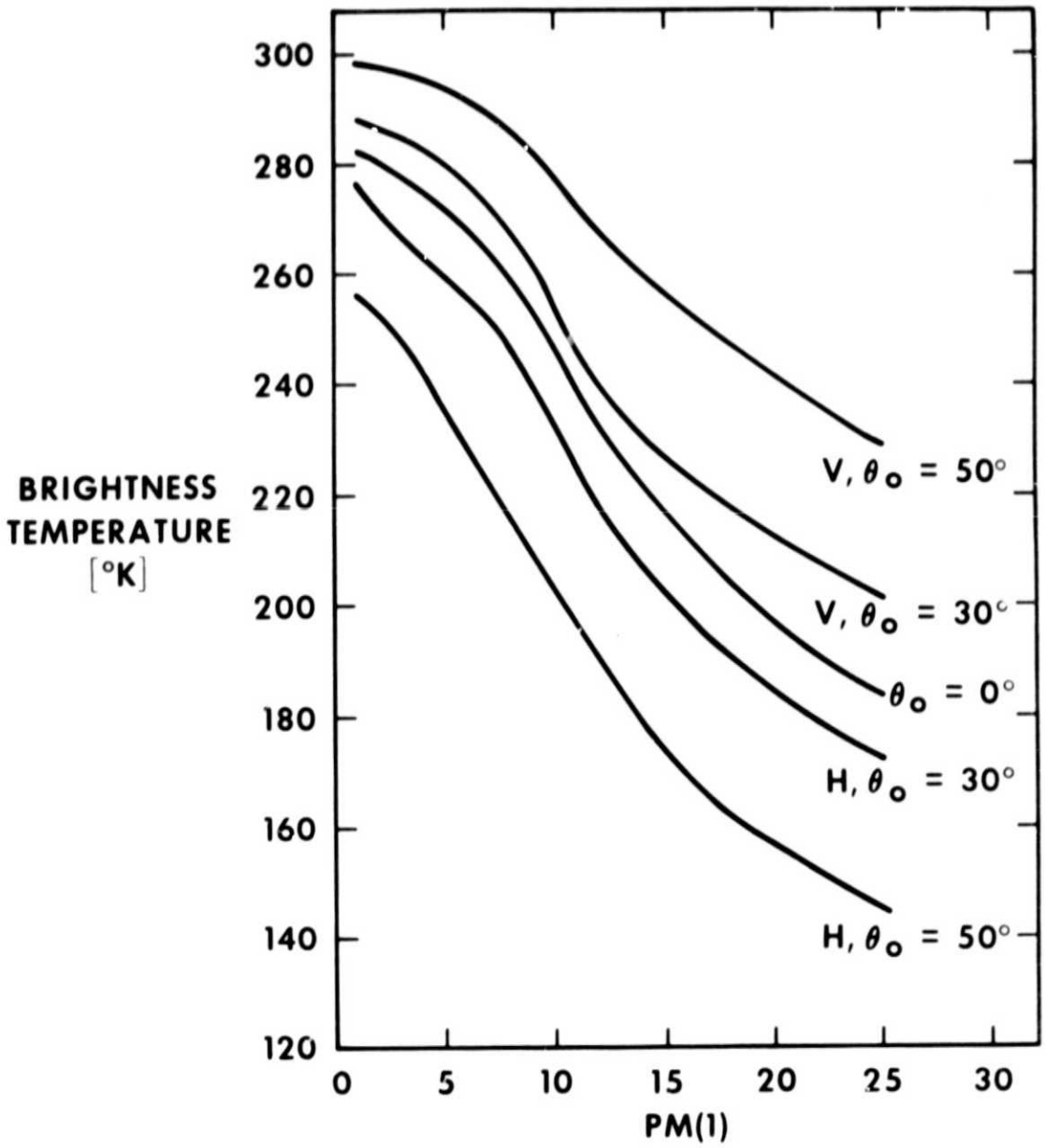

Figure 3.- Model calculations for vertical and horizontal polarizations at $\theta o = 0°$, $30°$ and $50°$ as a function of the percent moisture in the top layer of soil.

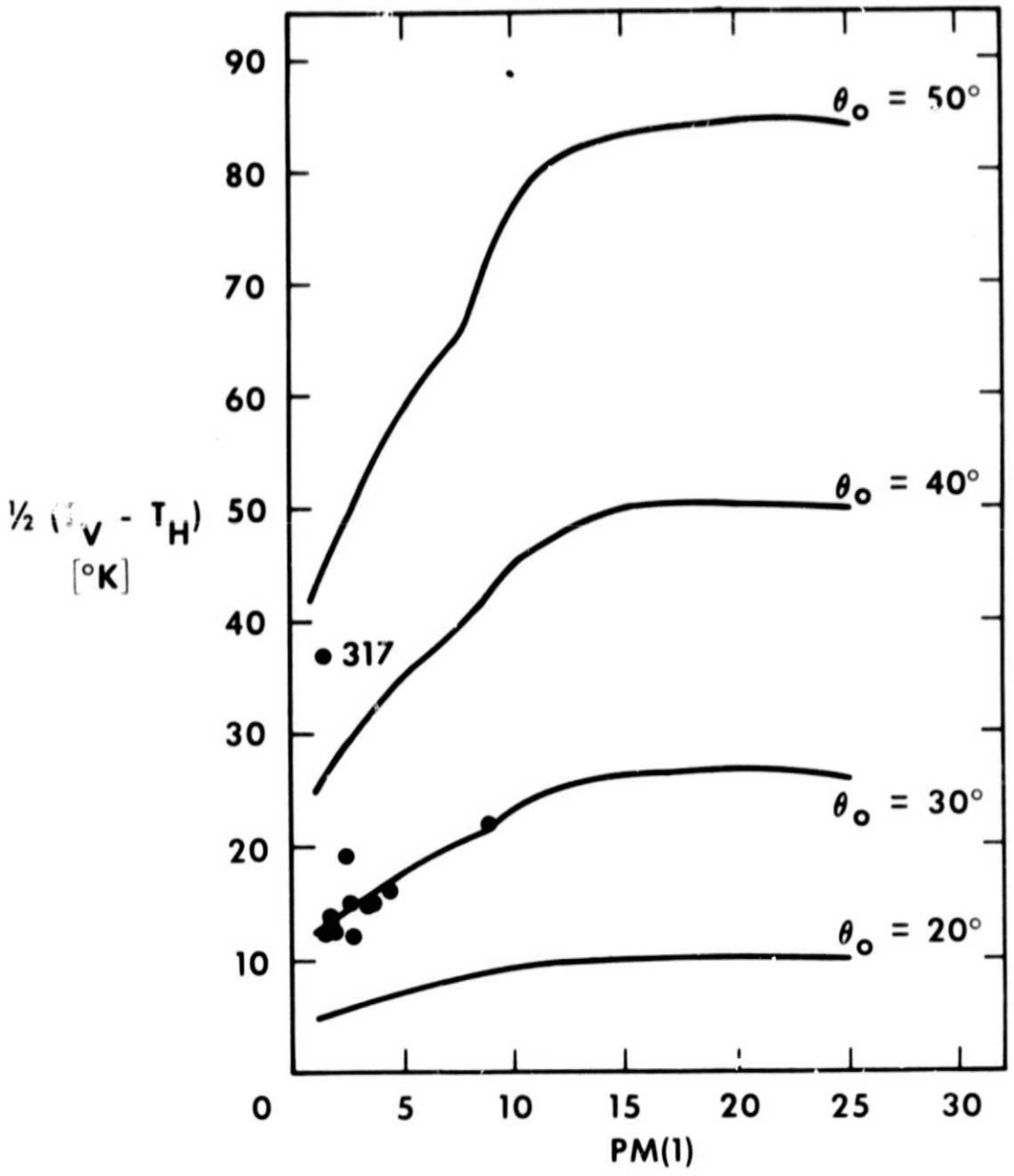

Figure 4.- Difference between predicted vertical and horizontal polarization brightness temperature for $\theta o = 20°$, $30°$, $40°$ and $50°$ as a function of the percent moisture in the top layer.

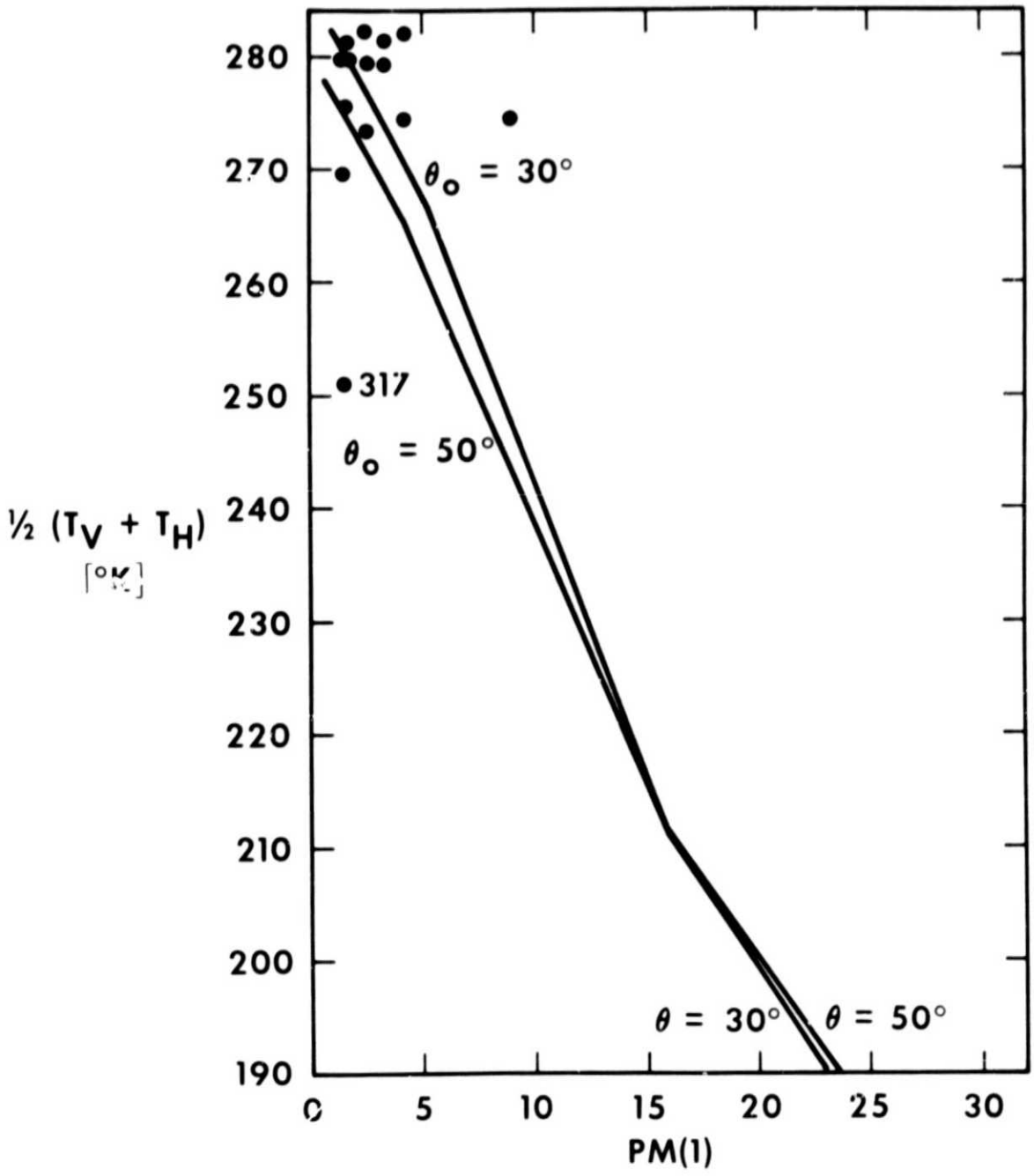

Figure 5.- The average of the predicted vertical and horizontal polarization brightness temperatures for $\theta o = 30^{\circ}$ and 50° as a function of the percent moisture in the top layer.

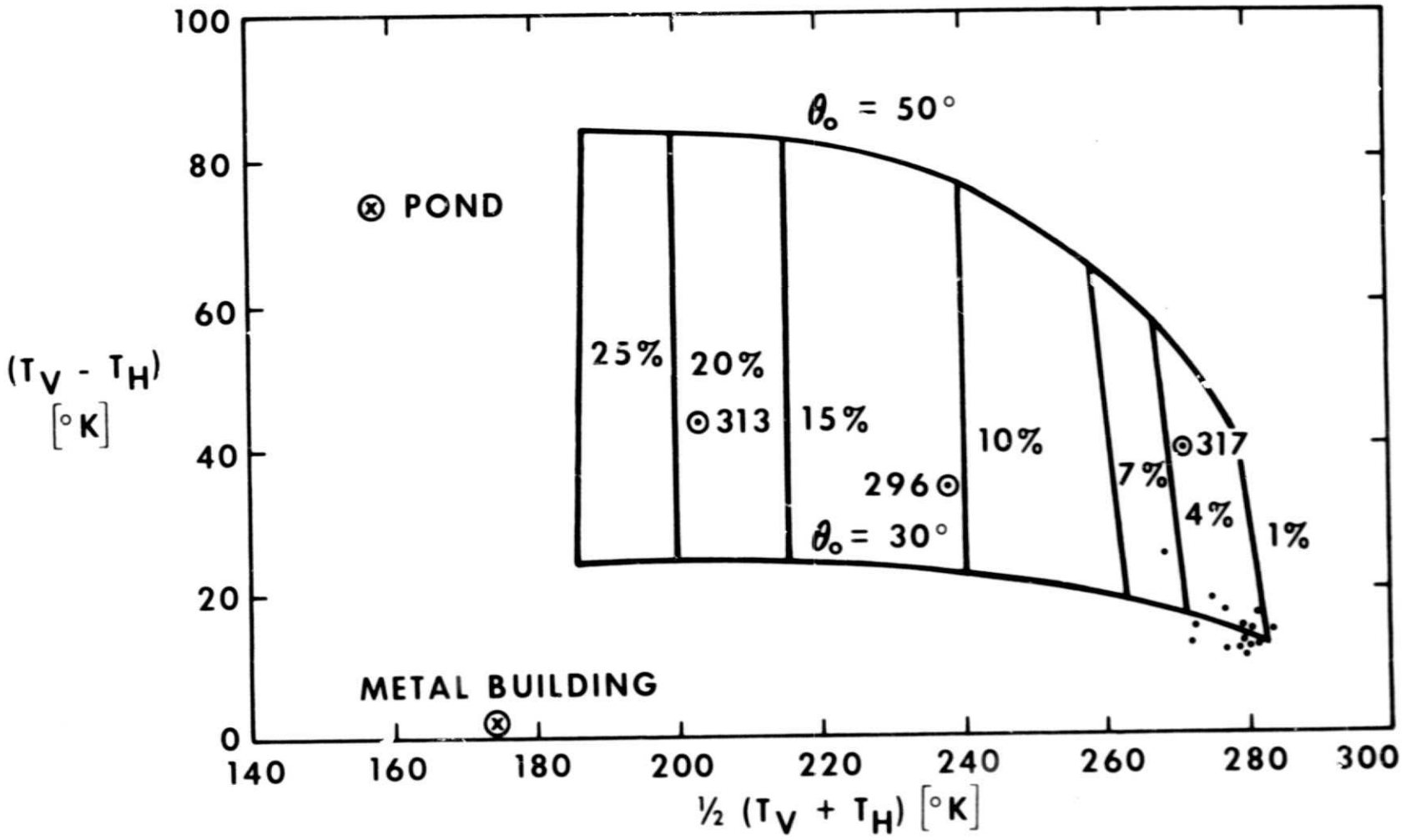

Figure 6.- The difference between predicted brightness temperatures at vertical and horizontal polarization as a function of their average for θo = 30° and 50°. The straight lines are lines of constant moisture in the top layer.

The model provides a means of knowing from what depth the radiation reaching the antenna comes. Figure 7 gives the contributions from the first, second, third, and fourth layers as a function of PM(1) for the ordinary profile. The contribution from the first layer is greatest for PM(1) = 11 percent. Although the radiation generated in this layer increases with increasing moisture, the fraction allowed to escape decreases. Output calculations were made with different moisture gradients. Contributions from the first three layers as a function of PM(2) are plotted on Figure 8. Beside each curve is the percent moisture in the first layer. Although the contributions from the first and second layers increase with increasing PM(2), the output from the third layer monotonically decreases. The sum of the contributions, except in the case of very dry crusts, allows little information about the actual gradient that gets through. In fact it is impossible to distinguish between cases in which PM(1) = 1 percent, PM(2) = 20 percent from PM(1) = 4 percent, PM(2) = 6 percent even though the average moisture over the top two centimeters is quite different. For PM(1) > 10 percent information about lower layers is completely lost. Perhaps, the ambiguity noted by Schmugge (ref. 1) for average moisture of < 10 percent can be partially explained in terms of the model's predictions.

APPLICATION OF THE MODEL TO MFMR DATA

Because the dielectric coefficients at L band frequencies of all of the soil types of the Phoenix area are not available, it is impossible to compare model prediction directly with MFMR data. However, an indirect attempt has been made using available T_V and T_H data for the April 5 flight. This attempt was in the form of a scatter plot of $T_V - T_H$ as a function of soil moisture. Preliminary results were not encouraging. Part of the difficulty arises from the fact that the aircraft flew north on line 1 and south on line 2 while making T_V measurements. The opposite directions were flown while making T_H observations. Thus on line 1 we observed the cold side of ridges measuring T_V and hot side measuring T_H, and vice versa on line 2. The effect is to diminish $(T_V - T_H)$ observation on line 1 and enhance them on line 2. Sun angle effects on the parameter $(T_V + T_H)/2$ should cancel.

As an example of this sun-angle effect consider observations made in Fields 11 and 13. The soil of both fields is sandy clay loam. The moisture profiles were similar and state of cultivation of the fields was identical. The temperatures observed in field 11 (line 2) were $T_V = 292.1$ and $T_H = 273.3$, while for field 13 (line 1) $T_V = 289.6$ and $T_H = 276.1$. A similar systematic dimunition and enhancement of $(T_V - T_H)$ is found in all of the lines 1 and 2 observations. Evidence for a sun angle effect is also obvious in the lines 3 and 4 data but to a lesser extent due to the fact that the midday sun was shining almost directly out of the south. The average values of $T_V - T_H$ and $(T_V + T_H)/2$ for the four flight lines (Table III) show an enhancement of the polarization difference along lines 2 and 4 and a dimunition along lines 1 and 3. Within a standard deviation, the intensity is the same along the four flight lines.

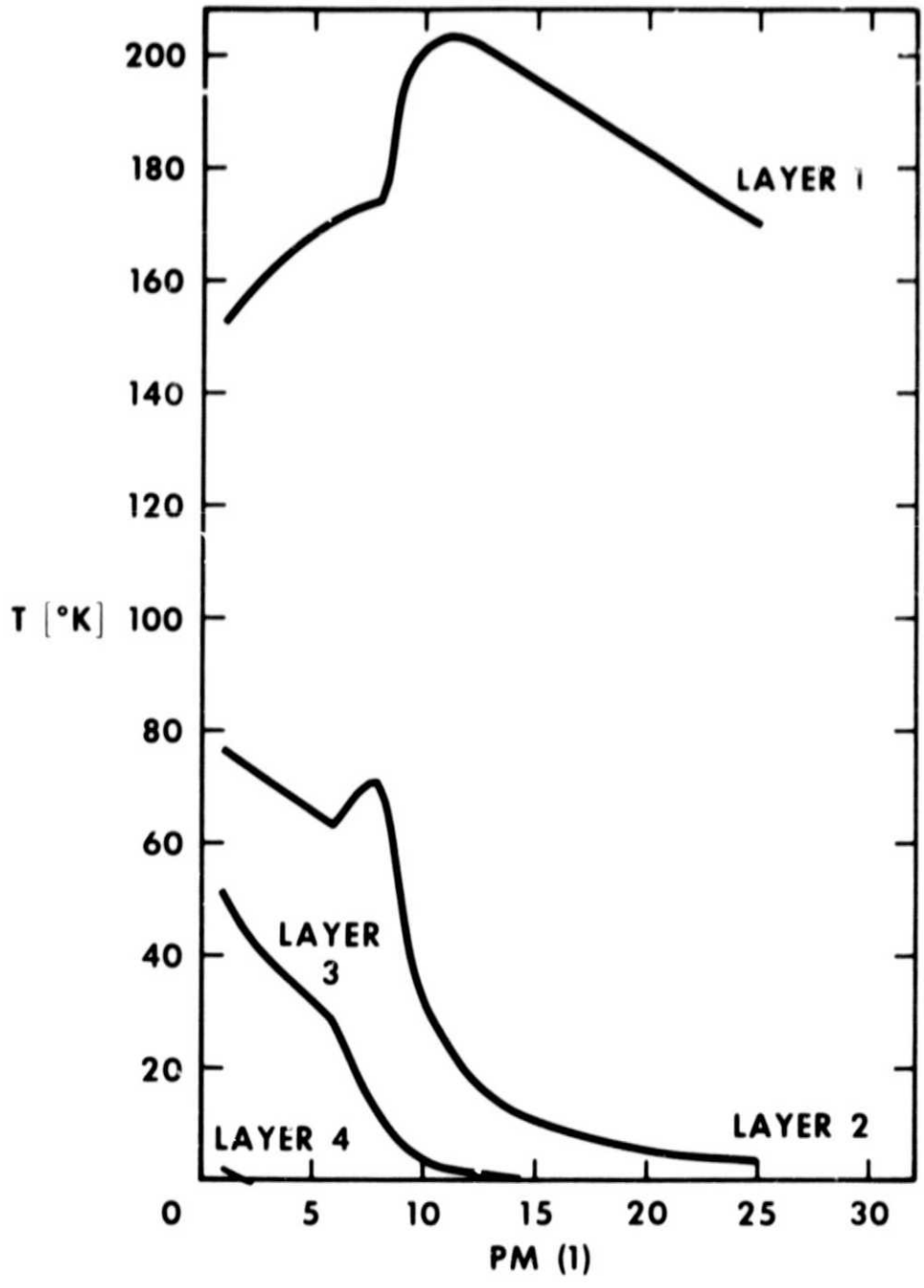

Figure 7.- The predicted brightness temperature contributions from the first, second, third and fourth layers at $\theta_c = 0^\circ$ as a function of the percent moisture in the top layer.

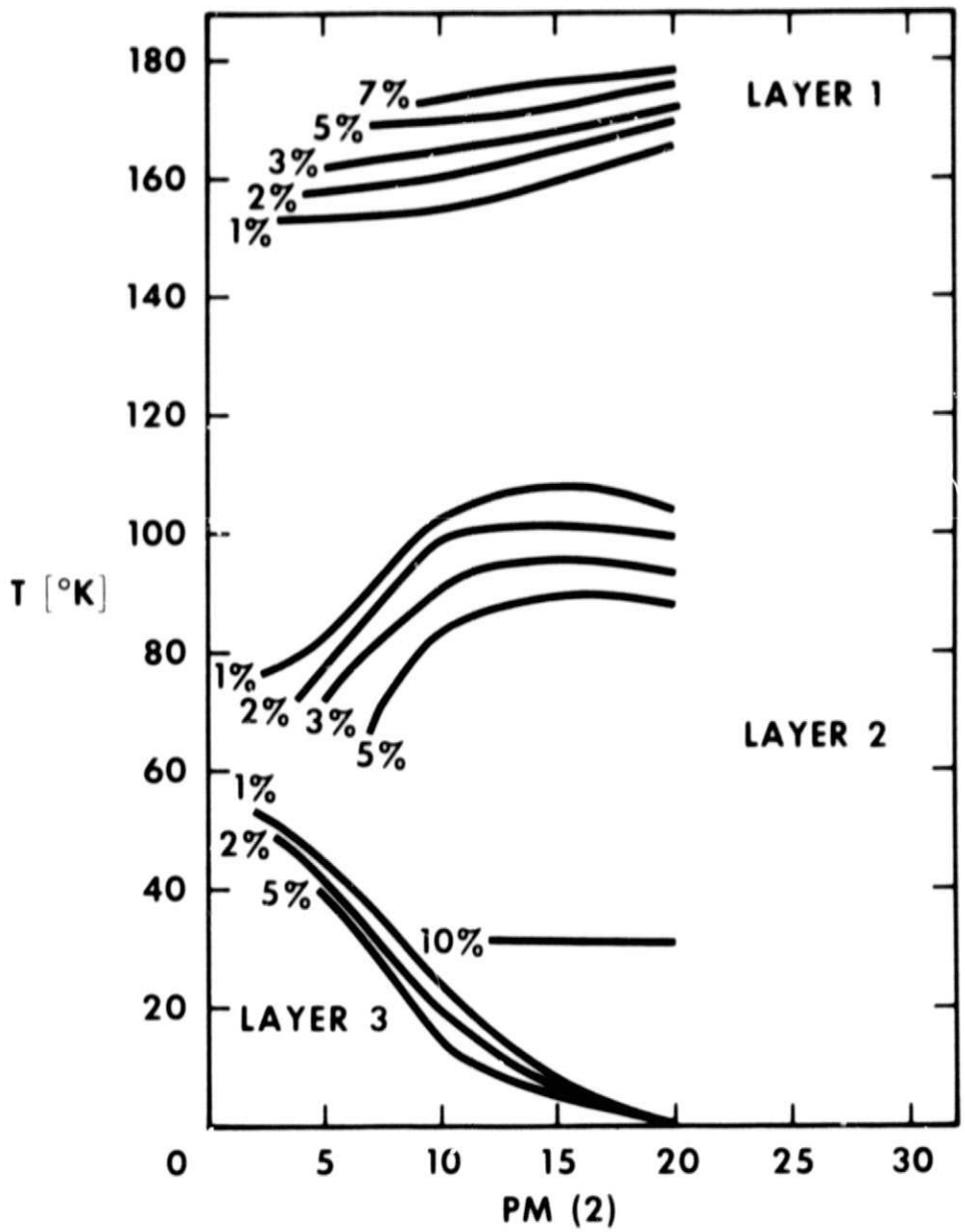

Figure 8.- Predicted brightness temperature contributions from the first second and third layers as a function of the percent moisture in the second layer. The look angle is 0°. The percent moisture in the top layers are also indicated.

TABLE III.- AVERAGE VALUES: G $T_V - T_H$ AND $(T_V + T_H)/2$

FOR FOUR FLIGHT LINES

Line	$T_V - T_H$	$(T_V + T_H)/2$
1	9.9 ± 2.3	283.8 ± 2.3
2	19.6 ± 4.4	278.4 ± 9.9
3	11.2 ± 4.7	283.8 ± 3.5
4	16.7 ± 5.2	281.2 ± 5.6

Another pertubation comes from the scales of roughness. It is the relatively large facets that contribute most to X band emission. Pending further analysis of the roughness scales, it seems quite reasonable to expect that large scale roughness at X band may turn out to be small and middle scale at L band. This is not to say that the model is inapplicable, rather that it has not been applied. Also the application in the analysis of data may be far more subtle than the X band application.

CONCLUSION

The radiative transfer equation to the problem of microwave emissions from layered, moist soils were applied. The predictions of the model were compared with a small set of X band observations and it was shown that:

1. Except for the case of flat surfaces the effect of surface roughness is to change the effective look angle from 50° to 30°

2. The predicted slope for nadir look is consistent with previously reported observations (Schmugge et al, 1974)

3. The model can be inverted to give the percent moisture in the top layer

The third conclusion does not preclude the possibility of gaining information about moisture in lower layers. We doubt that it can be known with the accuracy that we have of the top layer's moisture content.

One final result which deserves some stress concerns the role of the parameters $1/2(T_V + T_H)$ and $(T_V - T_H)$. We have seen that these are the components of the summed, radiatively transferred Stokes vectors. The distribution of points on Figure 8 suggests that these parameters can be used to make

maximum use of polarization information contained in the PMIS data by way of field classification. A cursory look of PMIS imagery suggests that these parameters can be exploited to classify various agricultural scenes.

The paper has not presented our model as new. Rather using well established principles, it has suggested heuristic methods by which information contained in microwave data may be exploited to enhance our understanding of this remote sensing technique.

APPENDIX

PROGRAM FOR BRIGHTNESS TEMPERATURES

```
      DIMENSION DEGREE(10), TH1(10), TH2(10),TV1(10),TV2(10)
      DIMENSION TCT(5),TCB(5),TCCT(5),TCCB(5)
      DIMENSION Z(7),DZ(7),PM(7,2),T(7,2),EPSR(7,2),EPSI(7,2),B(10,7,2),
     1          A(10,7,2),G(10,7,2),X(10),Y(10,7,2)
      DIMENSION R(10,7,2),SUM(10,7,2),RRH(10,7,2),TRV(10,7,2),TBH(10,7,2
     1),TBV(10,7,2),RH(10,7,2),RV(10,7,2),PMB(5,2)
      COMPLEX EPS(7,2),  CRV(10,7,2), RHOH(10,7,2),  RHOV(10,7,2)
      INTEGER BAND
      DATA  Z(1),Z(2),Z(3),Z(4),Z(5),Z(6),Z(7)/0.0,-1.0,-2.0,-5.0,-9.0,
     1      -15.0,-1.E6/
      DATA  DZ(1),DZ(2),DZ(3),DZ(4),DZ(5),DZ(6),DZ(7)/0.0,1.0,1.0,3.0,
     1      4.0,6.0,1.E6/
      DATA  PI/3.141592654/
      READ (5,1000)BAND
 1000 FORMAT(I5)
C       ENTER FIELD NUMBER, SOIL TYPE, MOISTURE AND TEMPERATURE PROFILES
      READ(5,39)(TCT(I),TCB(I),I=1,5)
   39 FORMAT(10F5.1)
    1 READ(5,2) FN,KST,((PMB(I,J),I=1,5),J=1,2)
    2 FORMAT(A5,I5,10F5.1)
C       FN = FIELD NUMBER
C       KST= SOIL TYPE
C    THE QUANTITY PMB IS THE AVERAGE PERCENT MOISTURE FOUND IN
C    BLANCHARD'S GROUND TRUTH BOOK
C       PM(I,J)= PERCENT MOISTURE IN ITH LAYER
C         T(I,J)= TEMPERATURE MEASURED IN ITH LAYER
C              J = 1 SAMPLE FROM TOP OF FURROW
C              J = 2 SAMPLE FROM BOTTOM OF FURROW
C           KST = 1   SANDY CLAY LOAM
C           KST = 2   CLAY LOAM
C           KST = 3   SANDY CLAY
C           KST = 4   CLAY
C IF BAND IS 1 WE ARE USEING L BAND  2 IS FOR X BAND
C  INITIALIZE NEEDED MATRICES
      DO 183 J=1,2
      DO 183 I=1,7
      DO 183 K=1,10
      PM(I,J)=0.0
   41 T(I,J)=0.0
      TH1(K)=0.0
      TH2(K)=0.0
      TV1(K)=0.0
      TV2(K)=0.0
      EPSR(I,J)=1.0
      EPSI(I,J)=0.0
      EPS(I,J)= CMPLX  (EPSR(I,J),EPSI(I,J))
      SUM(K,I,J) = 0.0
   76 B(K,I,J) = 1.0
      TRH(K,I,J) = 1.0
  105 TRV(K,I,J) = 1.0
      RHOH(K,I,J)=(0.0,0.0)
      RHOV(K,I,J)=(0.0,0.0)
      RH(K,I,J) = 0.0
      RV(K,I,J) = 0.0
      TBH(K,I,J) = 0.0
  183 TBV(K,I,J) = 0.0
C  BECAUSE THE SOIL TEMPERATURES WERE READ IN FROM BOTTOM TO TOP
C IT IS NECESSARY TO INVERT THE TEMPERATURE VECTOR.  THE CORRECTED
C  VECTOR IS GIVEN THE NAME TCCT OR TCCB.
      TCCT(1)=TCT(5)
      TCCT(2)=TCT(4)
```

```
      TCCT(3)=TCT(3)
      TCCT(4)=TCT(2)
      TCCT(5)=TCT(1)
      TCCB(1)=TCB(5)
      TCCB(2)=TCB(4)
      TCCB(3)=TCB(3)
      TCCB(4)=TCB(2)
      TCCB(5)=TCB(1)
      DO 42 J=1,2
   42 T(1,J)=30.0
      DO 43 I=2,6
      T(I,1) =T(I,1) +TCCT(I-1) + 273.0
   43 T(I,2) = T(I,2) +TCCB(I-1) + 273.0
      DO 46 J=1,2
      DO 46 I=2,6
   46 PM(I,J)=PMB(I-1,J)
      DO 44 J=1,2
      PM(7,J)=PM(6,J)
   44 T(7,J)=T(6,J)
      GO TO (250,251),BAND
  251 GO TO (3,4,5,5),KST
    3 DO 73 J=1,2
      DO 73 I=2,7
   86 IF(PM(I,J)-5.0)13,23,23
   13 EPSR(I,J)=2.5+0.2472*PM(I,J)
      EPSI(I,J)=0.42
      GO TO 73
   23 EPSR(I,J)=3.431-0.259*PM(I,J)+0.069*PM(I,J)**2-0.001*PM(I,J)**3
      EPSI(I,J)=2.207-0.659*PM(I,J)+0.065*PM(I,J)**2-0.001*PM(I,J)**3
   73 EPS(I,J)= CMPLX  (EPSR(I,J),EPSI(I,J))
      GO TO 100
    4 DO 74 J=1,2
      DO 74 I=2,7
   88 IF(PM(I,J)-8.0)14,24,24
   14 EPSR(I,J)=5.0+0.11425*PM(I,J)
      EPSI(I,J)=0.75
      GO TO 74
   24 EPSR(I,J)=-3.172+1.165*PM(I,J)-0.022*PM(I,J)**2+0.0003*PM(I,J)**3
      EPSI(I,J)=-5.385+1.007*PM(I,J)-0.034*PM(I,J)**2+0.0005*PM(I,J)**3
   74 EPS(I,J)= CMPLX  (EPSR(I,J),EPSI(I,J))
      GO TO 100
    5  DO 75  J=1,2
      DO 75 I=2,7
   90  IF(PM(I,J)-8)15,25,25
   15  EPSR(I,J)=2.5+0.325*PM(I,J)
       EPSI(I,J)=0.5+0.08*PM(I,J)
       GO TO 75
   25  EPSR(I,J)=-6.181+1.758*PM(I,J)-0.052*PM(I,J)**2+0.001*PM(I,J)**3
       EPSI(I,J)=-6.321+1.264*PM(I,J)-0.048*PM(I,J)**2+0.0008*PM(I,J)**3
   75 EPS(I,J)= CMPLX  (EPSR(I,J),EPSI(I,J))
      GO TO 100
  250 DO 91 J=1,2
      DO 91 I=2,7
      EPSR(I,J)=2.712+0.8036*PM (I,J)-0.1313*PM (I,J)**2
     1 +0.007619*PM (I,J)**3-0.000117*PM(I,J)**4
      EPSI(I,J)=-0.08975+0.2486*PM (I,J)-0.03569*PM (I,J)**2
     1 +0.001892*PM (I,J)**3 -0.00002720*PM (I,J)**4
   91 EPS(I,J)=CMPLX(EPSR(I,J),EPSI(I,J))
```

```
C      IN THIS PART OF THE PROGRAM THE VALUES OF THE REAL AND IMAGINARY
C     1PARTS OF THE WAVE VECTOR AS WELL AS THE EXTINCTION COEFFICIENT
C     2ARE CALCULATED AS A FUNCTION OF THE ANGLE OF EMERGENCE.
  100 DO 64 J=1,2
      DO 64 I=1,7
      DO 64 K=1,10
      DEGREE(K) = FLOAT(K-1)*10
      X(K)=DEGREE(K)*PI/180.0
      Y(K,I,J)=EPSR(I,J)-SIN(X(K))**2
      B(K,I,J)=SQRT(0.5*Y(K,I,J)*(1+SQRT(1+(EPSI(I,J)/(Y(K,I,J)))**2)))
      A(K,I,J)=EPSI(I,J)/(2.0*B(K,I,J))
      IF (BAND-1) 111,111,112
  111 G(K,I,J)=0.6*A(K,I,J)
      GO TO 64
  112 G(K,I,J)=4.48*A(K,I,J)
   64 CWV(K,I,J) =CMPLX  (B(K,I,J),A(K,I,J))
      DO 261 J=1,2
      DO 261  I=1,6
      DO 261 K=1,10
      RHOH(K,I,J)=(CWV(K,I,J)-CWV(K,I+1,J))/(CWV(K,I,J)+CWV(K,I+1,J))
      RH(K,I,J) = CABS(RHOH(K,I,J))**2
      RHOV(K,I,J)=(EPS(I,J)*CWV(K,I+1,J)-EPS(I+1,J)*CWV(K,I,J))/(EPS(I,
     1J)*CWV(K,I+1,J)+EPS(I+1,J)*CWV(K,I,J))
  261 RV(K,I,J) = CABS(RHOV(K,I,J))**2
C     CALCULATE THE TRANSMISSION FACTOR FOR H AND V POLARIZATIONS
C     CALCULATE THE WEIGHTING FUNCTION, W(K,I,J)
      DO 81 J=1,2
      DO 81 I=2,7
      DO 81 K=1,10
      DO 81 M=2,1
       TRH(K,I,J) = TRH(K,I,J)*(1.0 - RH(K,M-1,J))
   82  TRV(K,I,J) = TRV(K,I,J)*(1.0 -RV(K,M-1,J))
      SUM(K,I,J) = SUM(K,I,J) + G(K,M-1,J)*DZ(M-1)
   81 W(K,I,J) = EXP(-SUM(K,I,J))
C     CALCULATE THE BRIGHTNESS TEMPERATURE
      DO 83 J=1,2
      DO 83 K=1,10
      TBH(K,1,J)= T(1,J)*RH(K,1,J)
   83 TBV(K,1,J)= T(1,J)*RV(K,1,J)
      DO 84 J=1,2
      DO 84 I=2,7
      DO 84 K=1,10
      TBH(K,I,J)= TBH(K,I,J) + T(I,J)*W(K,I,J)*TRH(K,I,J)*(1.0-EXP(-G(K,
     1          I,J)*DZ(I)))*(1.0+RH(K,I,J)*EXP(-G(K,I,J)*DZ(I)))
      TBV(K,I,J)= TBV(K,I,J) + T(I,J)*W(K,I,J)*TRV(K,I,J)*(1.0-EXP(-G(K,
     1          I,J)*DZ(I)))*(1.0+RV(K,I,J)*EXP(-G(K,I,J)*DZ(I)))
   84 CONTINUE
      DO 99  K=1,10
      I = 1
  159 TH1(K)=TH1(K)+TBH(K,I,1)
      TH2(K)=TH2(K)+TBH(K,I,2)
      TV1(K)=TV1(K)+TBV(K,I,1)
      TV2(K)=TV2(K)+TBV(K,I,2)
      I = I+1
      IF(I.LE.7) GO TO 159
   99 CONTINUE
      WRITE(6,331)
  331 FORMAT(1H1,'      FN      KST     BAND      PH       T        ',)
```

ORIGINAL PAGE IS
OF POOR QUALITY

```
      WRITE(6,450)FN,KST,BAND
  450 FORMAT(A5,2I6)
      WRITE(6,133)
  133 FORMAT(1X,//)
      WRITE(6,455)  PM,T
  455 FORMAT(7F11.1/)
       WRITE(6,830)
  830 FORMAT(1H1,'          THH              TBV       ',)
      WRITE(6,132)
  132 FORMAT(1X,//)
      WRITE(6,810) TBH,TBV
  810 FORMAT(7(10E11.5/)//)
      WRITE(6,158)
  158 FORMAT(1H1,'     TH1       TH2       TV1       TV2       ')
      WRITE(6,134)
  134 FORMAT(1X,//)
      WRITE(6,71)TH1,TH2,TV1,TV2
   71 FORMAT     (10E11.5/)
      GO TO 1
      END
```

COMPILATION:

REFERENCES

1. Schmugge, T., P. Gloersen, T. Wilheit and F. Geiger, Remote Sensing of Soil Moisture with Microwave Radiometers, J. Geophys Res. 79, 313, 1974.

2. McAllum, W. E., Passive Microwave Imaging System Performance Evaluation, Johnson Space Center TM X-58109, 1973.

3. Reid, S., Multifrequency Microwave Radiometer (MFMR) L-Band Modification, Lockheed Electronics Co./Johnson Space Center, Document LEC - 036, 1973, JSC 09876.

4. Ulaby, F. T., A. K. Fung and S. Wu, The Apparent Temperature and Emissivity of Natural Surfaces at Microwave Frequencies, Technical Report 133-112 Center for Research, University of Kansas, 1970.

5. Paris J. F., Transfer of Thermal Microwave in the Atmosphere, Texas A&M PhD Dissertation, 1971.